ACS OMEGA

http://pubs.acs.org/journal/acsodf

Article

Electronic Mechanism of Martensitic Transformation in Nb-doped NiTi Alloys: A First-Principles Investigation

Xiaolan Yang and Jiaxiang Shang*

Cite This: *ACS Omega* 2021, 6, 22033−22038

Read Online

ACCESS | Metrics & More | Article Recommendations

ABSTRACT: The effect of Nb on the crystal structures and electronic mechanism of martensitic transformation in $Ni_{50}Ti_{50-x}Nb_x$ alloys is investigated by first principles. The lattice parameters, the formation energy, the middle eigenvalue of the transformation stretch tensor (λ_2), and the energy difference between the parent and martensite (ΔE) as a function of Nb content x (x = 0, 2.08, 6.25, 8.33, 10.42, 12.5, 18.75) are calculated. Lattice parameters increase with the increase of Nb content. The formation energies of the parent B2 phase, martensite orthorhombic B19, and monoclinic B19′ increase with the increase of Nb content. It is also found that at ≤10.42 at. % Nb, the martensite stable phase is monoclinic structure B19′; at >10.42 at. % Nb, the orthorhombic crystal structure B19 is formed. The energy difference between the parent and martensite means that the transformation temperature decreases with increasing Nb concentration at Nb ≤ 10.42 at. % and increases at >10.42 at. % Nb. The λ_2 of the NiTiNb alloys have the same value of about 0.95 with low Nb content. Furthermore, the electronic structure mechanisms behind the martensitic transformations are discussed in detail based on the density of states.

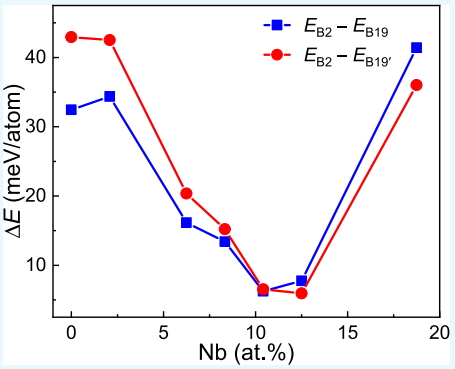

INTRODUCTION

Nitinol (NiTi) shape memory alloys (SMAs) have found wide applications in the biomedical industry and other technological areas because of their unique shape memory effect and superelasticity.[1,2] Recently, Lang et al. have discovered the two previously unreported phases for the binary $NiTi_2$ and Ni_5Ti compositions using structural search methods and ab initio calculations.[3] The martensitic phase transformation in NiTi was studied by the ab initio and Landau theoretical analysis.[4] The structural, thermal, and mechanical properties of the SMA NiTi are investigated from first-principles simulations.[5] Because of the very low yield strength of NiTi in the martensite state, the application of NiTi alloys as a high-strength damping material has been limited. NiTiNb SMAs have received considerable attention in recent decades owing to their excellent shape memory effect, high damping capacity, good mechanical properties, sufficient corrosion resistance, and wide transformation hysteresis, which have potential for a wide range of engineering applications such as pipe coupling or sealing.[6−13]

As a matter of fact, the phase transformation and mechanical properties are closely interrelated, which play an important role in the various applications of SMAs.[2,12−14] Zhao et al. reported experimentally that Nb can effectively enhance the yield stress, damping capacity, and hysteresis as well as change the transformation temperatures in NiTiNb SMAs.[8−12] They suggested that the martensite start temperature (M_s) is controllable through adjusting the Nb content and Ni/Ti ratio in NiTiNb alloys.[11] Moreover, the yield strength of NiTiNb alloys with low Nb content at room temperature increases with the increase of Nb content.[11] They summarized that at a lower Nb content, the Nb solid solution mechanism plays a primary role in affecting the yield strength of NiTiNb alloys.[9] However, at a higher Nb content, the yield strength of NiTiNb alloys is mainly affected by the β-Nb phase.[9] The presence of Nb either as a β-Nb phase or as a solution can enhance the transformation hysteresis.[11] Cui et al. observed a strong correlation between the size of thermal hysteresis (ΔT) and the middle eigenvalue (λ_2) of the transformation stretch tensor in the Ni−Ti−Cu thin film using the combinatorial approach, provided by the geometric non-linear theory of martensite (GNLTM).[15] Zhang et al.[16] verified the same correlation in the TiNiX alloys with X = Pd, Pt, Au. Furthermore, the phase compatibility between austenite and martensite in the $Ti_{50}Ni_{50-x}Pd_x$ bulk alloys by transmission electron microscopy was investigated.[17] The relationship between thermal hysteresis ΔT and λ_2 was identified in the quaternary Ti−Ni−Cu−Pd SMAs.[18] However, to the best of

Received: May 18, 2021
Accepted: August 10, 2021
Published: August 19, 2021

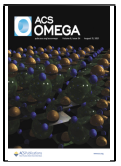

our knowledge, no systemic theoretical research about the martensitic transformations (MTs) of NiTiNb alloys has been conducted currently. Hence, based on our previous first-principles studies on the MTs of $Ti_{50}Ni_{50-x}Cu_x$ and $Ni_{50}Ti_{50-x}Zr_x$ SMAs,[19] the purpose of this work is to exploit the effect of Nb on the MT temperature and hysteresis of ternary NiTiNb alloys theoretically with different Nb contents.

RESULTS AND DISCUSSION

Crystal Structures of $Ni_{50}Ti_{50-x}Nb_x$ SMAs. The unit cells of NiTi B2, B19 orthorhombic, and B19′ monoclinic structures are shown in Figure 1. Here, the parent body-centered

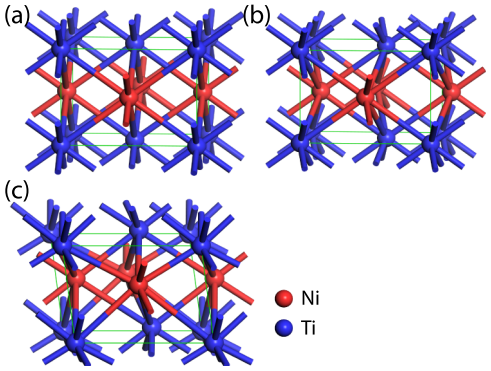

Figure 1. Initial unit cells of NiTi: (a) austenite lattice; (b) orthorhombic B19 martensite; (c) monoclinic B19′ martensite. Red spheres are Ni atoms; blue spheres are Ti atoms.

tetragonal (bct) lattice is employed. The lattice parameters of bct are $a = a_0$, $b = c = \sqrt{2}a_0$; here, a_0, is the structural parameter of the cubic B2 NiTi structure. The research indicated that the supercell approach is widely used in the doping study.[20] Since there are two sublattices in NiTi, we should first determine on which of the two sublattices the alloying elements are located. Indeed, according to experiments and calculations,[21] in Nb-doped NiTi, the Nb atoms occupy the Ti sublattice. Considering the symmetry of the cell, the crystal structures of B2 (bct), B19, and B19′ of $Ni_{50}Ti_{50-x}Nb_x$ with x = 0, 2.08, 6.25, 8.33, 10.42, 12.5, 18.75 are taken as the 3 × 2 × 2 B2 (bct), B19, and B19′ NiTi supercells, respectively, in which appropriate Ti are replaced by Nb.

Our previous study shows that the calculated lattice parameters of B2 (bct), B19, and B19′ are in good agreement with the experimental and theoretical data.[19,22−26] The computed lattice parameters of NiTi are a = 3.002 Å, b = 4.245 Å, c = 4.245 Å for B2 (bct); a = 2.739 Å, b = 4.242 Å, c = 4.633 Å for B19; and a = 2.913 Å, b = 4.081 Å, c = 4.647 Å for B19′.

It is reported that the size of the atoms and the number of valence electrons of the materials will affect the unit cell volumes in the intermetallic crystals.[27] In ternary $Ni_{50}Ti_{50-x}Nb_x$ alloys, the valence electrons per atom are calculated as

$$\frac{e_v}{a}Ni_{50}Ti_{50-x}Nb_x = \frac{50}{100}e_v^{Ni} + \frac{50-x}{100}e_v^{Ti} + \frac{x}{100}e_v^{Nb} \quad (1)$$

where e_v^{Ni}, e_v^{Ti}, and e_v^{Nb} are the numbers of valence electrons of Ni, Ti, and Nb, respectively, that is, e_v^{Ni} = 10, e_v^{Ti} = 4, and e_v^{Nb} = 5, and the Ni-$3d^8 4s^2$, Ti-$3d^2 4s^2$, and Nb-$4d^4 5s^1$ states are treated as valence states.[20,28,29] Since the number of valence electrons of Nb is slightly higher than that of Ti, the number of valence electrons per atom of TiNiNb increases slightly with increasing Nb content. Because Nb and Ti have similar valence states, the incorporation of Nb has a minimal effect on the unit

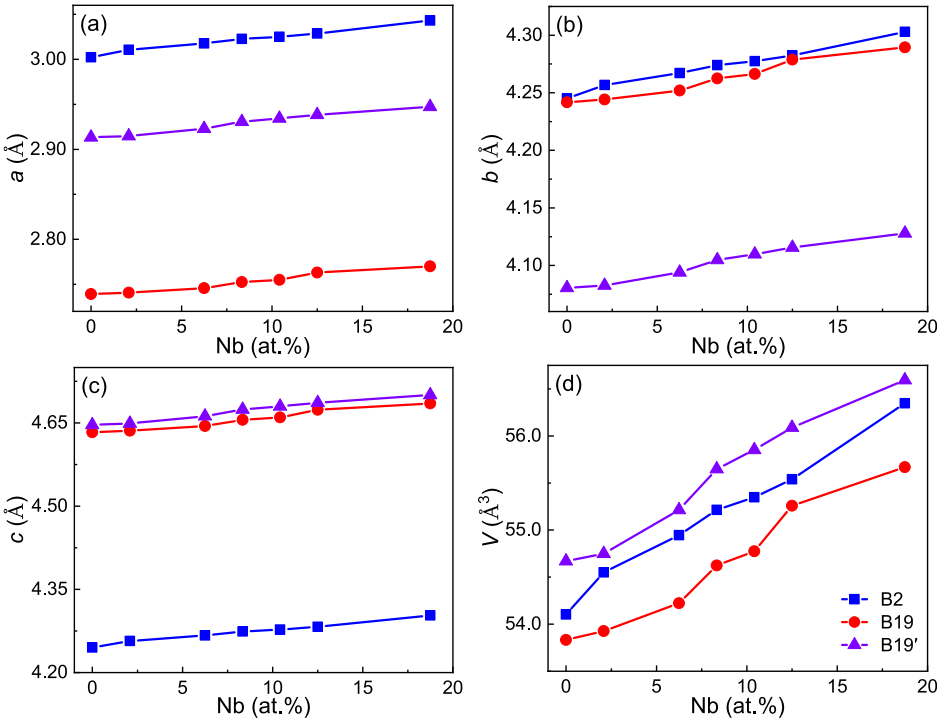

Figure 2. Compositional dependence of (a) "a" lattice parameter, (b) "b" lattice parameter, (c) "c" lattice parameter, and (d) unit cell volume in the $Ni_{50}Ti_{50-x}Nb_x$ alloys.

https://doi.org/10.1021/acsomega.1c02601
ACS Omega 2021, 6, 22033−22038

cell volumes of the $Ni_{50}Ti_{50-x}Nb_x$ alloys. In Figure 2, we present the lattice parameters of $Ni_{50}Ti_{50-x}Nb_x$ alloys as a function of Nb content. It can be seen that *a*, *b*, *c*, and unit cell volumes increase slightly with increasing Nb concentration. The marginally greater of unit cell volumes is mostly caused by a slightly larger atomic size of Nb compared with Ti and the larger valence electrons per atom.

Phase Stability of Ternary $Ni_{50}Ti_{50-x}Nb_x$ Alloys. Before explaining the strong compositional dependence of the phase-transition temperature of $Ni_{50}Ti_{50-x}Nb_x$ alloys using density functional theory (DFT), we study the MT path of $Ni_{50}Ti_{50-x}Nb_x$ alloys as a function of Nb content. In order to explore the phase stability of B2, B19, and B19′ structures in ternary NiTiNb alloys, we invoke the formation energies, E_{form}.[30−32] All these energies are normalized per atom. E_{form} is calculated as

$$E_{form} = E(Ni_{50}Ti_{50-x}Nb_x) - \frac{50}{100}E(Ni) - \frac{50-x}{100}E(Ti) - \frac{x}{100}E(Nb) \quad (2)$$

with $E(Ni_{50}Ti_{50-x}Nb_x)$ being the total energy per atom of the TiNiNb alloys and E(Ni), E(Ti), and E(Nb) being the total energies per atom of face-centered cubic (fcc) Ni, hexagonal close-packed (hcp) Ti, and body-centered cubic (bcc) Nb in their elemental state, respectively.

The corresponding energies of formation calculated according to eq 2 are plotted in Figure 3. It can be found

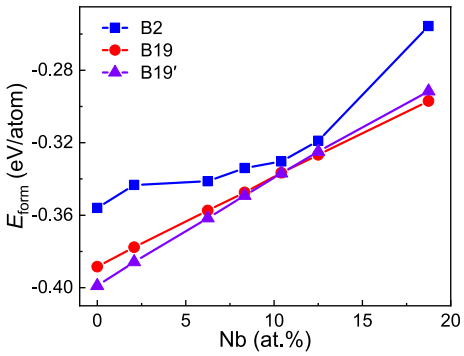

Figure 3. Energy of formation E_{form} per atom as a function of Nb content in the $Ni_{50}Ti_{50-x}Nb_x$ alloys.

that in the binary NiTi alloy, the B19 phase is lower in formation energy than the B2 phase; the monoclinic structure B19′ is the NiTi martensitic phase with the lowest formation energy. These calculations are in line with earlier reported experimental and theoretical results.[19,23,33]

As presented in Figure 3, the formation energies of all the phases increase with increasing Nb substitution, which means that the B2, B19, and B19′ structures become less stable with increasing Nb content in TiNiNb alloys. E_{form} of the B2 phase is much higher than that of martensite phases all the time with increasing Nb concentration. This reveals that the martensite phase is more stable compared with the B2 phase, which is in accordance with the experimental observations that the martensite phase is the lower-temperature phase.

The results shown in Figure 3 demonstrate a crossover at the formation energy curve for Nb = 10.42 at. % concentration. For Nb ≤ 10.42 at. %, the stable martensite phase is the monoclinic B19′ structure, with a lower E_{form} than the B19 structure, while for Nb > 10.42 at. %, the stable martensite is the B19 phase with an orthorhombic structure due to the lowest E_{form}. This means that there are two types of transformation paths: at low Nb content, MT is B2 to B19′; at high Nb content, the B2 to B19 path would be observed. To our knowledge, no experimental or theoretical studies have proposed the martensitic phase stability of NiTiNb alloys.

The calculated density of states (DOS) of austenite B2 and martensite B19′ phases for $Ni_{50}Ti_{50-x}Nb_x$ alloys is shown in Figure 4. For both B2 and B19′ NiTi, it can be observed that

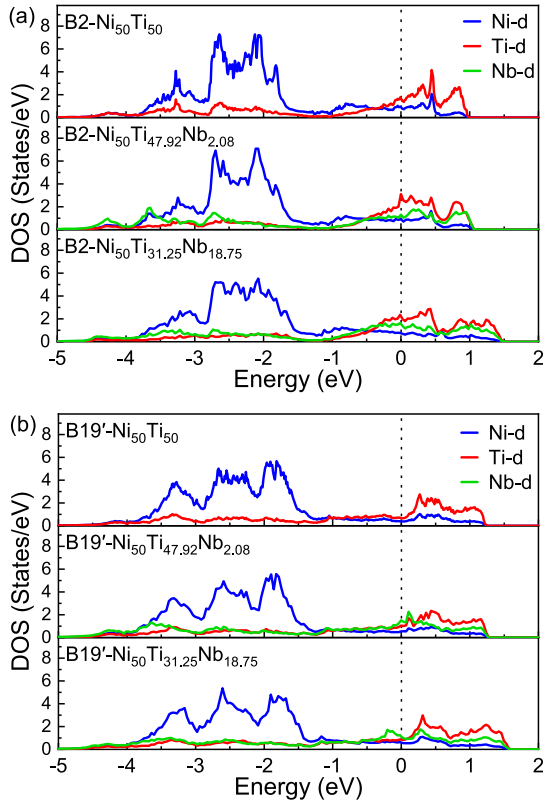

Figure 4. DOSs of the (a) austenite B2 and (b) martensite B19′ phases for $Ni_{50}Ti_{50-x}Nb_x$ alloys. The Fermi level is located at 0 eV.

the DOSs below and above the Fermi level are mainly due to the Ni d and Ti d states, respectively, which is consistent with the analysis of DOSs in other literature studies.[34] Furthermore, compared to B2 NiTi, the peak positions of B19′ shift to lower energies and the hybridizations between Ti d and Ni d states are stronger in the energy region of −4 to −3 eV. It is indicated that B19′ is the martensitic stable structure in the binary NiTi alloy, which is in agreement with the energy calculation shown in Figure 3.

With the increase of the Nb concentration, for the DOSs of B2 and B19′ $Ni_{50}Ti_{50-x}Nb_x$ serials, the peak positions of Ni atoms and Ti−Nb resonated atoms shift to a higher energy slightly. DOSs of the Nb-d state increase near the Fermi level and decrease at a lower energy level. Therefore, the stabilities of both B2 and B19′ phases slightly decrease with the increase of Nb content, which is consistent with the analysis of E_{form} (see Figure 3). For the same composition, the DOSs of B2 at a lower energy level (−4 to −3 eV) are lower and sharper than that of B19′, while the DOSs of B19′ at a higher energy level (−3 to −1.5 eV) are wider. This means that the B19′ structure

https://doi.org/10.1021/acsomega.1c02601
ACS Omega 2021, 6, 22033−22038

is more stable than the B2 structure for the same NiTiNb composition, which is consistent with the energy results.

Compositional Dependence of Martensite Start Temperatures of TiNiNb Alloys. After obtaining the phase stability by means of calculating the E_{form}, we set out to rationalize the effects of alloy composition on M_s in TiNiNb alloys theoretically. Here, we invoke the total energy differences,[31] ΔE, which are defined (per atom) as the total energy per atom of austenite minus that of the martensite structure, that is,

$$\Delta E_{B19} = E_{B2} - E_{B19} \quad (3)$$

and

$$\Delta E_{B19'} = E_{B2} - E_{B19'} \quad (4)$$

The calculated ΔE_{B19} and $\Delta E_{B19'}$ of binary NiTi are 32 and 43 meV atom^{-1}, respectively. The present calculations are in good agreement with previously reported data.[19,22,23,26,35] We can note that $\Delta E_{B19'} > \Delta E_{B19} > 0$, which indicates that B19′ is the most stable one, the same in the section of E_{form} mentioned above.

The corresponding ΔE_{B19} and $\Delta E_{B19'}$ of $Ni_{50}Ti_{50-x}Nb_x$ alloys (obtained from the 3 × 2 × 2 supercells) are plotted in Figure 5 as a function of the Nb content. The results

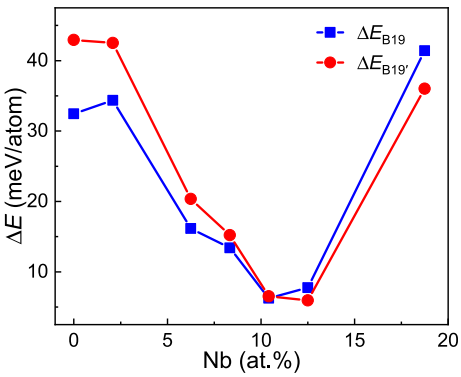

Figure 5. Dependence of energy differences between austenite and martensite on Nb concentration in $Ni_{50}Ti_{50-x}Nb_x$ alloys.

presented in Figure 5 clearly show that there is a crossover at the ΔE curve for Nb contents about 11 at. %. For Nb contents <10.42 at. %, we find $\Delta E_{B19'} > \Delta E_{B19} > 0$, which demonstrates that both B19 and B19′ phases are lower in energy than the high-temperature austenite B2 phase, and the monoclinic B19′ phase possesses the lowest energy. Nevertheless, for Nb > 12.5 at. %, $\Delta E_{B19} > \Delta E_{B19'} > 0$, and the ΔE_{B19} is higher than $\Delta E_{B19'}$, which suggests that orthorhombic B19 is a martensite phase of the lowest energy. These data points presented in Figure 5 further suggest that the two ΔE curves come closer with increasing Nb content; however, for Nb > 12.5 at. %, they come further with the increase of Nb. This reveals that the B19 phase may exhibit better stability than the B19′ phase for Nb concentrations exceeding the critical point at which the two ΔE curves cross each other. The relative stability of B19 and B19′ structures is changed by the incorporation of Nb into NiTi. This is confirmed by the calculations of E_{form} (see Figure 3).

The ΔE of the most stable phase versus composition for $Ni_{50}Ti_{50-x}Nb_x$ alloys is replotted in Figure 6. The trend shows that the alloy composition at 10.42 at. % of niobium exhibits

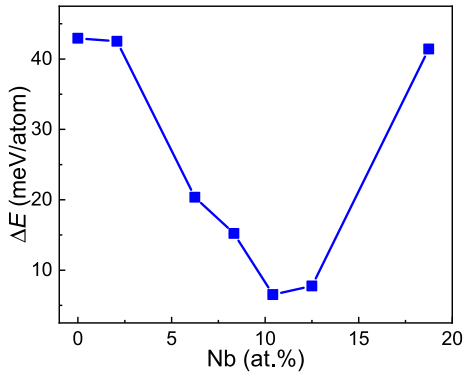

Figure 6. Influence of alloy composition on ΔE for $Ni_{50}Ti_{50-x}Nb_x$ alloys.

the lowest values of ΔE. One sees two lines shaped like a V. This plot suggests that the addition of Nb leads to a smaller ΔE and subsequently to a lower M_s temperature. The martensite start temperature (M_s), austenite start temperature (A_s), and $A_s - M_s$ of NiTiNb alloys from previous experimental work are listed in Table 1.[8,12] It can be found from Table 1 that the present calculation results are mainly consistent with earlier reported experimental data.

Table 1. Martensite Start Temperature (M_s), Austenite Start Temperature (A_s), and $A_s - M_s$ of NiTiNb Alloys from Previous Experimental Work

alloys	M_s (°C)	A_s (°C)	$A_s - M_s$ (°C)	refs
$Ni_{50}Ti_{50}$	58	88	30	8
$Ni_{50}Ti_{49}Nb_1$	50	75	25	12
$Ni_{50}Ti_{48}Nb_2$	16	38	22	12
$Ni_{50}Ti_{47}Nb_3$	−43	−11	32	12
$Ni_{49.6}Ti_{45.9}Nb_{4.5}$	−77	−48	29	12
$Ni_{49.8}Ti_{45.2}Nb_5$	−100	−65	35	12
$Ni_{47}Ti_{44}Nb_9$	−73	−25	48	12
$Ni_{41}Ti_{44}Nb_{15}$	23	56	33	8

Effects of Nb on the Transformation Thermal Hysteresis. The following concerns the thermal hysteresis of NiTiNb SMAs accompanied with the martensitic phase transformations. The energy dissipation during transformation, in the form of thermal hysteresis, can be reduced by increasing the phase compatibility between martensite and austenite. According to GNLTM, the transformation stretch tensor U derived by the lattice parameters of both the austenite and martensite phases for a cubic-to-orthorhombic transformation is[15,17,36]

$$U_1 = \begin{bmatrix} \beta & 0 & 0 \\ 0 & \frac{\alpha-\gamma}{2} & \frac{\alpha+\gamma}{2} \\ 0 & \frac{\alpha+\gamma}{2} & \frac{\alpha-\gamma}{2} \end{bmatrix} \quad (5)$$

where $\beta = \lambda_1 = a/a_0$, $\alpha = \lambda_2 = b/\sqrt{2}a_0$, and $\gamma = \lambda_3 = c/\sqrt{2}a_0$. The closer the middle eigenvalue of the transformation stretch tensor is to 1, the better the compatibility. Several investigations indicate that thermal hysteresis achieved a minimum when the middle eigenvalue

https://doi.org/10.1021/acsomega.1c02601
ACS Omega 2021, 6, 22033−22038

was close to unity in the Ni−Ti−X alloy systems with X = Cu, Pd, Pt, and Au.[15−19]

We calculated the middle eigenvalue by $\lambda_2^{B19} = b_{B19}/b_{B2}$ using the lattice parameters of austenite B2 and orthorhombic martensite B19. For cubic-to-monoclinic transformation, λ_2 is calculated as $\lambda_2^{B19'} = b_{B19'}\sin\beta/b_{B2}$, where β is the monoclinic angle of the B19′ martensite. In Figure 7, we present the

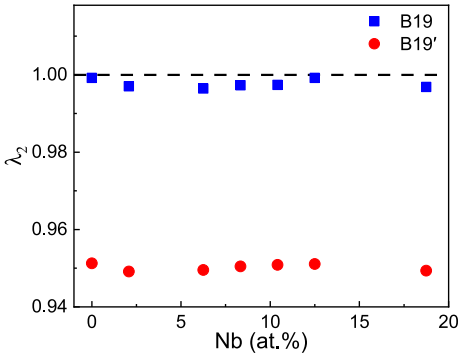

Figure 7. Variation of the middle eigenvalue, λ_2, with the Nb concentration in the Ni−Ti−Nb alloy system.

variations of the middle eigenvalue (λ_2) as a function of Nb content. The value of λ_2 varies slightly with the low content of Nb. Experimental results have shown that the hysteresis of $Ni_{49.6}Ti_{45.9}Nb_{4.5}$ is quite near that of binary NiTi SMAs (20−30 °C in general) (see Table 1).[12] It can be observed that low Nb content has little effect on the thermal hysteresis of NiTiNb. However, the wider hysteresis of $Ni_{47}Ti_{44}Nb_9$ (48 °C) should be ascribed to other factors, for example, the existence of a large amount of the β-Nb phase.

However, the effect of impurity to the NiTi alloy is not concerned in this research. Oxygen adsorption and diffusion on the NiTi alloy surface[37,38] and the corrosion behaviors of different Ni−Ti alloys[39] were investigated. The H defect in the NiTi alloy[40] and the microcosmic mechanism of carbon influencing on the $NiTiNb_9$ alloy[41] are presented. The oxidation resistance of TiNiNb alloys has been discussed.[13] Improving the oxidation or corrosion resistance of NiTi alloys is of great importance. We would further explore the effect of oxygen on the NiTiNb alloys using ab initio calculations.

CONCLUSIONS

First-principles calculations were performed to study the effect of Nb content on the martensitic phase transformation in $Ni_{50}Ti_{50-x}Nb_x$ (x = 0, 2.08, 6.25, 8.33, 10.42, 12.5, 18.75) SMAs. We can draw the following conclusions:

(1) Based on the geometrical optimizations, our results clearly show that the larger structure parameters as well as unit cell volumes are observed with the increase of Nb content.
(2) Present research has shown that at low Nb addition to NiTi alloys, the transformation path is B2 to the monoclinic phase, while at high Nb content, the transformation path is B2 to the orthorhombic structure in NiTiNb.
(3) Nb additions have been found to depress the martensite start temperature of NiTi alloys, which are in agreement with the experimental study.
(4) The thermal hysteresis of the TiNiNb alloys has very slight variations with low Nb content.

METHODS

Calculations employing the PW91[42] of generalized gradient approximation[43] functional were performed in the VASP[44−46] code with projector augmented wave[47] pseudopotentials and an energy cutoff of 500 eV, ensuring convergence of energy within 0.1 meV $atom^{-1}$, and the force on atoms is less than 0.01 eV/Å. The lattice optimization of all the possible doping structures was performed. Brillouin zone sampling was performed using a 4 × 4 × 4 special k-point mesh.[48]

AUTHOR INFORMATION

Corresponding Author

Jiaxiang Shang − *School of Materials Science and Engineering, Beihang University, Beijing 100191, China;* orcid.org/0000-0001-9923-4090; Email: shangjx@buaa.edu.cn

Author

Xiaolan Yang − *School of Materials Science and Engineering, Beihang University, Beijing 100191, China; School of Physics and Electronic Science, Zunyi Normal College, Zunyi 563006, China*

Complete contact information is available at: https://pubs.acs.org/10.1021/acsomega.1c02601

Funding

This research was funded by the National Natural Science Foundation of China (NSFC, grants nos. 51371017 and 11864047) and the Natural Science Foundation of Technology Department (QKHLH [2015]7021).

Notes

The authors declare no competing financial interest.

ACKNOWLEDGMENTS

The utilization of the computing facilities at the High Performance Computing Center (HPCC) of Beihang University is acknowledged.

REFERENCES

(1) Buehler, W. J.; Wiley, R. C. TiNi-ductile intermetallic compound. *ASM Trans.* **1962**, *55*, 269−276.
(2) Otsuka, K.; Ren, X. Physical metallurgy of Ti-Ni-based shape memory alloys. *Prog. Mater. Sci.* **2005**, *50*, 511−678.
(3) Lang, L.; Payne, A.; Valencia-Jaime, I.; Verstraete, M. J.; Bautista-Hernández, A.; Romero, A. H. Assessing Nickel Titanium Binary Systems Using Structural Search Methods and Ab initio Calculations. *J. Phys. Chem. C* **2021**, *125*, 1578−1591.
(4) Kumar, P.; Waghmare, U. V. First-principles phonon-based model and theory of martensitic phase transformation in NiTi shape memory alloy. *Materialia* **2020**, *9*, 100602.
(5) Haskins, J. B.; Lawson, J. W. Finite temperature properties of NiTi from first principles simulations: Structure, mechanics, and thermodynamics. *J. Appl. Phys.* **2017**, *121*, 205103.
(6) Li, K.; Li, Y.; Yu, K. Y.; Liu, C.; Gibson, D.; Leyland, A.; Matthews, A.; Fu, Y. Q. Crystal size induced reduction in thermal hysteresis of Ni-Ti-Nb shape memory thin films. *Appl. Phys. Lett.* **2016**, *108*, 171907.
(7) Li, K.; Li, Y.; Huang, X.; Gibson, D.; Zheng, Y.; Liu, J.; Sun, L.; Fu, Y. Q. Surface microstructures and corrosion resistance of Ni-Ti-Nb shape memory thin films. *Appl. Surf. Sci.* **2017**, *414*, 63−67.
(8) Bao, Z.-z.; Guo, S.; Xiao, F.; Zhao, X.-q. Development of NiTiNb in-situ composite with high damping capacity and high yield strength. *Prog. Nat. Sci.: Mater. Int.* **2011**, *21*, 293−300.

(9) Xiao, F.; Ma, G.; Zhao, X.; Xu, H. Effects of Nb Content on Yield Strength of NiTiNb Alloys in Martensite State. *Chin. J. Aeronaut.* **2009**, *22*, 658−662.
(10) Liu, W.; Zhao, X. Mechanical Properties and Transformation Behavior of NiTiNb Shape Memory Alloys. *Chin. J. Aeronaut.* **2009**, *22*, 540−543.
(11) Chen, Y.; Jiang, H.-c.; Rong, L.-j.; Xiao, L.; Zhao, X.-q. Mechanical behavior in NiTiNb shape memory alloys with low Nb content. *Intermetallics* **2011**, *19*, 217−220.
(12) Wang, M.; Jiang, M.; Liao, G.; Guo, S.; Zhao, X. Martensitic transformation involved mechanical behaviors and wide hysteresis of NiTiNb shape memory alloys. *Prog. Nat. Sci.: Mater. Int.* **2012**, *22*, 130−138.
(13) Zhao, X.; Xu, J.; Tang, L.; Gong, S. High temperature oxidation behavior of NiTiNb intermetallic alloys. *Intermetallics* **2007**, *15*, 1105−1115.
(14) Hu, Q. M.; Yang, R.; Lu, J. M.; Wang, L.; Johansson, B.; Vitos, L. Effect of Zr on the properties of (TiZr)Ni alloys from first-principles calculations. *Phys. Rev. B: Condens. Matter Mater. Phys.* **2007**, *76*, 224201.
(15) Cui, J.; Chu, Y. S.; Famodu, O. O.; Furuya, Y.; Hattrick-Simpers, J.; James, R. D.; Ludwig, A.; Thienhaus, S.; Wuttig, M.; Zhang, Z.; Takeuchi, I. Combinatorial search of thermoelastic shape-memory alloys with extremely small hysteresis width. *Nat. Mater.* **2006**, *5*, 286−290.
(16) Zhang, Z.; James, R. D.; Müller, S. Energy barriers and hysteresis in martensitic phase transformations. *Acta Mater.* **2009**, *57*, 4332−4352.
(17) Delville, R.; Kasinathan, S.; Zhang, Z.; Humbeeck, J. V.; James, R. D.; Schryvers, D. Transmission electron microscopy study of phase compatibility in low hysteresis shape memory alloys. *Philos. Mag.* **2010**, *90*, 177−195.
(18) Zarnetta, R.; Takahashi, R.; Young, M. L.; Savan, A.; Furuya, Y.; Thienhaus, S.; Maaß, B.; Rahim, M.; Frenzel, J.; Brunken, H.; et al. Identification of quaternary shape memory alloys with near-zero thermal hysteresis and unprecedented functional stability. *Adv. Funct. Mater.* **2010**, *20*, 1917−1923.
(19) Yang, X.; Ma, L.; Shang, J. Martensitic transformation of $Ti_{50}(Ni_{50-x}Cu_x)$ and $Ni_{50}(Ti_{50-x}Zr_x)$ shape-memory alloys. *Sci. Rep.* **2019**, *9*, 3221.
(20) Gou, L.; Liu, Y.; Ng, T. Y. An investigation on the crystal structures of $Ti_{50}Ni_{50-x}Cu_x$ shape memory alloys based on density functional theory calculations. *Intermetallics* **2014**, *53*, 20−25.
(21) Shi, H.; Frenzel, J.; Martinez, G. T.; Van Rompaey, S.; Bakulin, A.; Kulkova, S.; Van Aert, S.; Schryvers, D. Site occupation of Nb atoms in ternary Ni−Ti−Nb shape memory alloys. *Acta Mater.* **2014**, *74*, 85−95.
(22) Huang, X.; Ackland, G. J.; Rabe, K. M. Crystal structures and shape-memory behaviour of NiTi. *Nat. Mater.* **2003**, *2*, 307−311.
(23) Kibey, S.; Sehitoglu, H.; Johnson, D. D. Energy landscape for martensitic phase transformation in shape memory NiTi. *Acta Mater.* **2009**, *57*, 1624−1629.
(24) Kudoh, Y.; Tokonami, M.; Miyazaki, S.; Otsuka, K. Crystal-structure of the martensite in Ti-49.2at%Ni alloy analyzed by the single-crystal X-ray-diffration method. *Acta Metall.* **1985**, *33*, 2049−2056.
(25) Philip, T. V.; Beck, P. A. CsCl-type ordered structures in binary alloys of transition elements. *Trans. AIME J. Metals* **1957**, *9*, 1269−1271.
(26) Zhang, J. M.; Guo, G. Y. Microscopic Theory of the Shape Memory Effect in TiNi. *Phys. Rev. Lett.* **1997**, *78*, 4789−4792.
(27) Simon, A. Intermetallic Compounds and the Use of Atomic Radii in Their Description. *Angew. Chem., Int. Ed.* **1983**, *22*, 95−113.
(28) Zarinejad, M.; Liu, Y. Dependence of Transformation Temperatures of NiTi-based Shape-Memory Alloys on the Number and Concentration of Valence Electrons. *Adv. Funct. Mater.* **2008**, *18*, 2789−2794.
(29) Zarinejad, M.; Liu, Y.; White, T. J. The crystal chemistry of martensite in NiTiHf shape memory alloys. *Intermetallics* **2008**, *16*, 876−883.
(30) Alonso, P. R.; Rubiolo, G. H. Relative stability of bcc structures in ternary alloys with $Ti_{50}Al_{25}Mo_{25}$ composition. *Phys. Rev. B: Condens. Matter Mater. Phys.* **2000**, *62*, 237−242.
(31) Chen, J.; Li, Y.; Shang, J.; Xu, H. First principles calculations on martensitic transformation and phase instability of Ni-Mn-Ga high temperature shape memory alloys. *Appl. Phys. Lett.* **2006**, *89*, 231921.
(32) Holec, D.; Friák, M.; Dlouhy, A.; Neugebauer, J. Ab initio study of point defects in NiTi-based alloys. *Phys. Rev. B: Condens. Matter Mater. Phys.* **2014**, *89*, 014110.
(33) Otsuka, K.; Ren, X. Recent developments in the research of shape memory alloys. *Intermetallics* **1999**, *7*, 511−528.
(34) Tan, C.-L.; Cai, W.; Tian, X.-H. First-principles study on the effect of Hf content on martensitic transformation temperature of TiNiHf alloy. *Chin. Phys.* **2006**, *15*, 2718−2723.
(35) Ye, Y. Y.; Chan, C. T.; Ho, K. M. Structural and electronic properties of the martensitic alloys TiNi, TiPd, and TiPt. *Phys. Rev. B: Condens. Matter Mater. Phys.* **1997**, *56*, 3678.
(36) Ma, J.; Karaman, I.; Noebe, R. D. High temperature shape memory alloys. *Int. Mater. Rev.* **2010**, *55*, 257−315.
(37) Li, Y.-C.; Wang, F.-H.; Shang, J.-X. Ab initio study of oxygen adsorption on the NiTi(110) surface and the surface phase diagram. *Corros. Sci.* **2016**, *106*, 137−146.
(38) Liu, X.; Guo, H.; Meng, C. Oxygen Adsorption and Diffusion on NiTi Alloy (100) Surface: A Theoretical Study. *J. Phys. Chem. C* **2012**, *116*, 21771−21779.
(39) Ding, R.; Shang, J.-X.; Wang, F.-H.; Chen, Y. Electrochemical Pourbaix diagrams of Ni Ti alloys from first-principles calculations and experimental aqueous states. *Comput. Mater. Sci.* **2018**, *143*, 431−438.
(40) Moitra, A.; Solanki, K. N.; Horstemeyer, M. F. The location of atomic hydrogen in NiTi alloy: A first principles study. *Comput. Mater. Sci.* **2011**, *50*, 820−823.
(41) Li, G. F.; Lu, S. Q.; Dong, X. J.; Peng, P. Microcosmic mechanism of carbon influencing on $NiTiNb_9$ alloy. *J. Alloys Compd.* **2012**, *542*, 170−176.
(42) Perdew, J. P.; Chevary, J. A.; Vosko, S. H.; Jackson, K. A.; Pederson, M. R.; Singh, D. J.; Fiolhais, C. Atoms, molecules, solids, and surfaces: Applications of the generalized gradient approximation for exchange and correlation. *Phys. Rev. B: Condens. Matter Mater. Phys.* **1992**, *46*, 6671−6687.
(43) Perdew, J. P.; Wang, Y. Accurate and simple analytic representation of the electron-gas correlation energy. *Phys. Rev. B: Condens. Matter Mater. Phys.* **1992**, *45*, 13244−13249.
(44) Kresse, G.; Furthmüller, J. Efficient iterative schemes for ab initio total-energy calculations using a plane-wave basis set. *Phys. Rev. B: Condens. Matter Mater. Phys.* **1996**, *54*, 11169−11186.
(45) Kresse, G.; Furthmüller, J. Efficiency of ab-initio total energy calculations for metals and semiconductors using a plane-wave basis set. *Comput. Mater. Sci.* **1996**, *6*, 15−50.
(46) Kresse, G.; Hafner, J. Ab initio molecular dynamics for open-shell transition metals. *Phys. Rev. B: Condens. Matter Mater. Phys.* **1993**, *48*, 13115−13118.
(47) Kresse, G.; Joubert, D. From ultrasoft pseudopotentials to the projector augmented-wave method. *Phys. Rev. B: Condens. Matter Mater. Phys.* **1999**, *59*, 1758−1775.
(48) Monkhorst, H. J.; Pack, J. D. Special points for Brillouin-zone integrations. *Phys. Rev. B: Solid State* **1976**, *13*, 5188−5192.

https://doi.org/10.1021/acsomega.1c02601
ACS Omega 2021, 6, 22033−22038